DEMISE AND SURVIVABILITY CRITERIA FOR SPACECRAFT DESIGN OPTIMIZATION

Mirko Trisolini[(1)], Hugh G. Lewis[(2)], Camilla Colombo[(3)]

[(1)]University of Southampton, University road, Southampton, UK, Email: m.trisolini@soton.ac.uk
[(2)] University of Southampton, University road, Southampton, UK, Email: H.G.Lewis@soton.ac.uk
[(3)] University of Southampton, University road, Southampton, UK, Email: C.Colombo@soton.ac.uk

ABSTRACT

In a period where the evolution of the space environment is causing increasing concerns for the future of space exploitation and sustainability, the design for demise philosophy has gained an increased interest. However, satellites designed for demise still have to survive the space environment polluted by space debris. Within this context we are developing a model to evaluate the effect of preliminary design choices on the survivability and on the demise of a spacecraft configuration. Considering common spacecraft components such as tanks and batteries, a set of maps are presented, which shows the variation of survivability and demise criteria as function of the component geometry and material. Furthermore, a preliminary multi-objective optimization is performed to evaluate a simple spacecraft configuration and define an optimal design according to the demise and the survivability criteria.

1. INTRODUCTION

In the context of a sustainable use of the outer space, the major space faring nations and international committees [1-3] have proposed a series of debris mitigation measures, including the de-orbiting of spacecraft at the end of their operational life. The consequent growth of the ground casualty risk associated with the increased frequency of re-entering objects can be limited by designing a spacecraft through a design for demise philosophy, where most of the spacecraft will not survive the re-entry process. Such strategies may favor uncontrolled re-entry disposal options over the controlled ones, because a spacecraft will be more likely to meet the casualty risk requirements. This could make design for demise a simpler and cheaper alternative for the disposal of satellites at the end of their operational lives [4, 5]. However, a spacecraft designed to demise still has to survive for several years the space environment, which is populated by a large number of space debris and meteoroids. The impact with particles even of millimeter in size can be extremely dangerous for satellites and cause the loss of the mission [6-8]. This means that the spacecraft design has also to fulfill the requirement of survivability against on-orbit debris impacts. The demise and the survivability are both influenced by a set of common design choices such as the outer structure material, the geometry and the shape of the structure [4, 9]. Within this context, we developed two models to assess the demise and the survivability of a preliminary mission design concept. Two criteria are thus presented to evaluate the degree of demise and survivability of a spacecraft configuration against the different spacecraft and components design parameters. The link between the design parameters and the specific spacecraft components such as tanks and battery cells is also taken into account. In addition, mission characteristics such as the mission duration and operational orbit are taken into account, with a particular attention towards Earth observation missions and remote sensing missions. Results shows how spacecraft design parameters and mission constraints affect the design choices when considering the effects on the demise and survivability of a spacecraft.In a preliminary attempt to perform an optimization for the selection of the design parameters, the two developed models are used to construct the fitness functions in a multi-objective optimization framework. In this way, trade-off solutions that consider both the demise and survivability design drivers can be found. As the problem is nonlinear and involves the combination of continuous variable such as the thickness and the size of the objects together with discrete variables like the material type, classical derivative based procedures becomes unsuited. Thus a heuristic optimization approach based on genetic algorithms was selected. The optimization algorithm uses the demise and survivability models and criteria to evaluate possible design choices as function of the characteristics of the object. The solutions are presented as a Pareto front showing the best non-dominated individuals obtained from the evolved initial population.

It is important to consider demisability and survivability requirements since the early stage of the mission design process [5]. A late analysis of such requirements may cause an inadequate integration of these design practice, leading to late changes to the mission, which of course are more expensive and may cause delay in the mission timeline. On the other end, an early consideration of demise and survivability requirements can favor cheaper options such as the uncontrolled re-entry of the satellite, without losing survivability performance and, thus, mission reliability.

2. SURVIVABILITY AND DEMISE MODELS

To analyze spacecraft configurations and components against the demisability and the survivability requirements it is necessary to develop two separate models. The first model allows the user to perform a re-entry analysis of a simplified representation of a spacecraft and to evaluate its demise performance, the second model carries out a debris impact analysis and returns the penetration probability of the analyzed structure as a measure of its survivability during the mission lifetime. The two models are also used to compute the terms that composes the fitness function in a multi-objective optimization process. For this reason, throughout their development, much effort is made to maintain a comparable level of detail and computational time between them. A more detailed description of the model is presented in [10].

2.1. Demise Model

The demise model consists of an object-oriented code [11-14]. The main feature of object-oriented codes resides in the fast simulation of the spacecraft re-entry through the use of a simplified model of the spacecraft structure; this is achieved by reducing the satellite design and its components into primitive shapes (e.g. spheres, cubes). The re-entry trajectory simulation uses a three degree of freedom dynamics where only drag forces are considered (i.e. ballistic motion) whereas lift and thrust are neglected (i.e. uncontrolled re-entry). In doing so, the computation of the attitude motion of the object is not required, but assumed as random tumbling (in the case of the algorithm developed for this work). The adoption of motion and shape averaged drag coefficients allows determining the pressure forces on each component [12, 15-18]. The computation of the thermal load on the components uses the Detra-Kemp-Riddel correlation [19, 20] to obtain the hypersonic heat rate at each instant of the re-entry and a set of motion and shape averaged shape factor to adjust the heat load to the specific shape considered [15, 21-24].

The re-entry analysis also requires the knowledge of the gravity acceleration and of the Earth's atmosphere characteristics in order to simulate correctly the descent trajectory. The model of the Earth's gravitational potential is zonal harmonic gravity model up to degree 4 [25]. The atmospheric model employed is the 1976 U.S. Standard Atmosphere [26], as implemented by the Public Domain Aeronautical Software (PDAS) [27].

Another important aspect is the characteristics of the material considered. For our purposes, the materials have temperature independent properties, which have been obtained from the database of the Debris Assessment Software (DAS) [11].

The demise of an object, i.e. its mass loss during the re-entry, is analyzed with a lumped mass model where the temperature of the object remains uniform over the entire volume. After reaching the melting temperature, the object starts losing mass at a rate that is proportional to the net heat flux on the object and to the heat of fusion. The result of the demise simulation is here expressed in terms of an index called Residual Mass Fraction (RMF), which is defined as the ratio between the final mass at the end of the re-entry and the initial mass of the object as Eq. (1) shows.

$$RMF = \frac{m_{fin}}{m_{in}} \tag{1}$$

2.2. Survivability Model

The survivability model analyzes instead the satellite resistance against the impacts of untraceable space debris and meteoroids. The procedure involves representing the spacecraft structure with a panelized schematization of its shape. To each panel we assign a material selected from a predefined library and geometrical properties such as the type of shielding, the wall thickness and the failure modality (i.e. penetration, detached spall and incipient spall are possible options). The survivability model uses the same geometrical elementary shapes of the demise model to represent satellite structures, in order to keep the two models comparable. Beside the geometrical schematization of the satellite, a representation of the space environment is also needed. This is obtained using the European Space Agency (ESA) state of the art software MASTER-2009 [28] that provides a description of the debris environment via flux predictions on user defined target orbit. MASTER-2009 provides the impact fluxes with an impactor diameter between 0.0001 m and 0.1 m, and a set of 2D and 3D flux distributions as a function of the impact azimuth, impact elevation, impact velocity, and particle diameter. Then, we subdivide the space around the satellite in a set of angular sectors and associate to each sector a vector element containing the average of the impact flux, impact direction and impact velocity (see Figure 1).

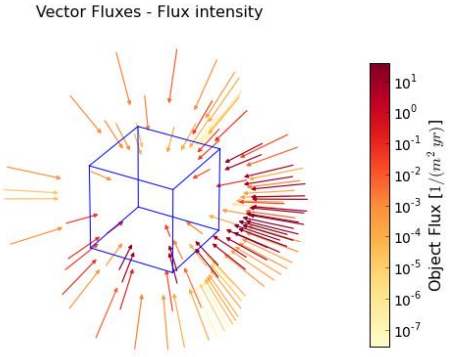

Figure 1. Vector flux elements

The code then uses the vector characteristics of impact flux, direction and velocity previously described to compute the critical diameter corresponding to each panel of the structure using Ballistic Limit Equations (BLEs).
Once obtained the critical diameter, the corresponding critical flux allows computing the penetration probability using Poisson statistics (see Eq. (2)).

$$P_{j,i}^{p} = 1 - e^{-\phi_{c,i} A_j^{\perp} t} \quad (2)$$

where the index j identifies the panel and the index i the vector flux. $\phi_{C,i}$ is the critical particle flux in 1/m^{2}yr that is the flux of particles having a diameter bigger than the computed critical diameter, $A_j^{\perp}$ is the projected area of the j-th face in the direction of the i-th vector flux and t is the mission duration in years.
The penetration probability ($P_{j,i}^{p}$) is computed in this way for each vector flux on every panel of the structure and then we compute the overall penetration probability (P^p) with Eq. (3) [29].

$$P^{p} = 1 - \prod_{j=1}^{N_{panels}} \left(\prod_{i=1}^{N_{fluxes}} \left(1 - P_{j,i}^{p}\right) \right) \quad (3)$$

where N_{panels} and N_{fluxes} are the number of panels in which the structure is schematized and the number of vector flux elements, respectively

3. SURVIVABILITY AND DEMISE MAPS FOR SATELLITE COMPONENTS

To have a better understanding of a combined demisability and survivability analysis, we present a set of contour maps showing the variation of the RMF (see Eq. (1)) and of the penetration probability (see Eq. (3)) as a function of the thickness, dimension and material of the object. In addition, the orbit characteristics for the survivability and the initial re-entry conditions for the demise are taken into account. Figure 2 shows an example of such contour maps for a cubic shaped object re-entering from an altitude of 120 km at a velocity of 7.3 km/s, with an operational orbit of 800 km of altitude and 98 degrees of inclination, for a mission lifetime of 3 years.
The x-axis and y-axis represent the thickness and the side length of the cube, respectively. The blue contour lines identify the RMF percentage of 1, 50 and 99 percent, meaning that an object with dimension under the 1 percent curve will have less than 1 percent of its mass remaining after the re-entry. The red contour lines, on the other hand, represent the 0.1, 1, and 10 percent penetration probability of a structure for the considered mission orbit and lifetime. The bottom right corner of the map (grey area) identifies a region of non-physical combination of thickness and side length that is when the thickness is greater than half the side length. The arrows indicate in which direction of the contour map the survivability and the demisability are improving. It is possible to observe that, as expected, an increased thickness results in a better survivability performance, whereas a thinner object will, in general, be more demisable. Both criteria instead favor smaller objects: for the survivability, a smaller cross-sectional area means a lower probability of getting impacted by space debris, and for the demisability, a smaller object is less massive and thus in general easier to demise. Of course also physical constraints need to be taken into account as, for example, the overall size of a spacecraft can be strongly influenced by the dimensions of the payload.

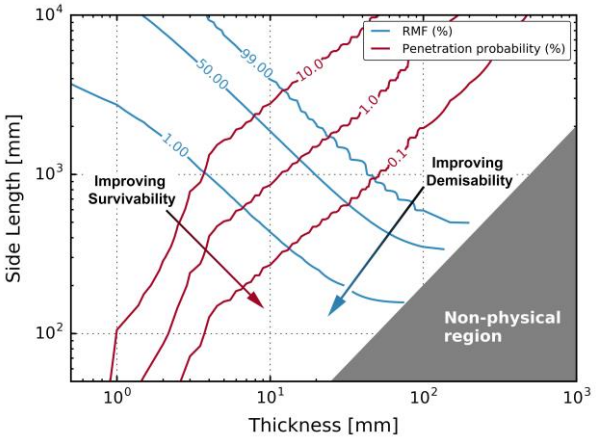

Figure 2. Combined survivability and demisability map

A set of results are here presented taking Earth observation and remote sensing missions as an example. Many of these missions exploit sun-synchronous orbits due to their favorable characteristics that allow the spacecraft to pass over any given point of the Earth's surface at the same local time. Examples of this kind of missions are Landsat 8 [30], MetOp [31] SPOT 6/7 [32] and many others. As already pointed out, sun-synchronous orbits have highly appealing features for Earth observation mission, and for this reason, they are much exploited. An indication about the current population of satellites populating the sun-synchronous region is represented in Figure 3. Figure 3 shows the current population of satellite between an altitude of 400 and 800 km and an inclination between 0 and 150 degrees (data from [33]). Each point represents a satellite, and it is possible to observe a very high concentration of satellites around the 98 degrees inclination. The number of satellites is even higher than it appears from the figure since the points superimpose each other because of the very similar inclinations of the satellites. The plot also includes a color-map showing the penetration probability on an aluminum alloy (7075-T6) cube of 1-meter side length and 4 mm thickness as a function of the orbital inclination and altitude. As it can

be observed, the sun-synchronous region is not only very populated, but it is also one if not the most exposed to the debris environment with the highest penetration probability. Following these considerations, a set of three circular orbits with altitude of 600, 700, and 800 kilometers respectively and an inclination of 98 degrees were selected (see Figure 4). In fact, these orbital altitudes and inclination enclose many of the operational orbits of the previously cited sun-synchronous missions. Earth observation and remote sensing missions usually have a lifetime of at least 3 years, and up to 10 years.

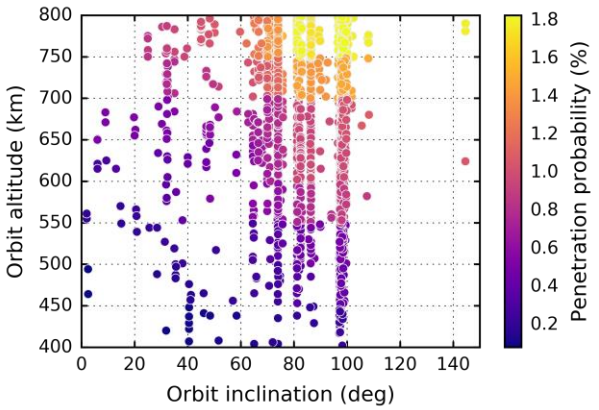

Figure 3. Satellite distribution for orbit between 0 and 150 degrees of inclination and 400 and 800 km of altitude, with associated esteem of their penetration probability

This consideration led to the decision of taking into account 4 different mission durations of 3, 5, 7, and 10 years respectively (see Figure 5).
The difference among the different orbits considered is observable in Figure 4 and it is caused by the different amount of space debris populating the selected orbits.

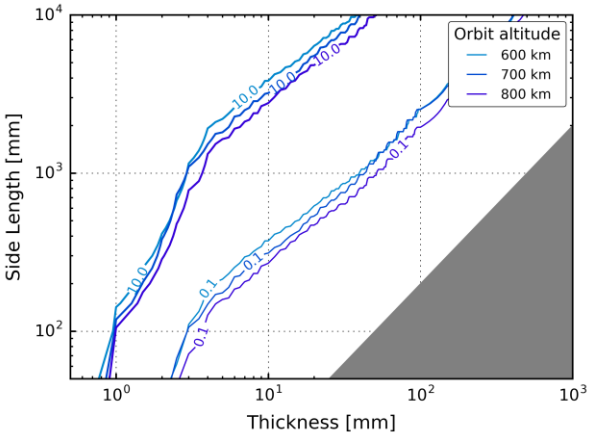

Figure 4. Penetration probability as function of orbit altitude (orbit inclination of 98 degrees)

The 800 km orbit has the highest particle density thus producing greater impactor fluxes, which in turn translate into a higher penetration probability on a structure.
On the other end, as expected, an extended mission lifetime results in a higher penetration probability. From Figure 5 the trend appears to be linear with correspondent penetration probability lines almost equally spaced as the mission duration varies.

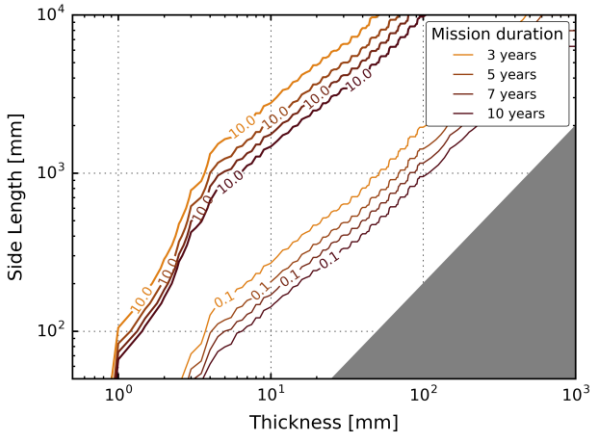

Figure 5. Penetration probability as function of mission duration

A consideration can be done on where the main spacecraft structures and components are located inside these maps; in other words, which are the usual ranges of thickness and size of common spacecraft components. We represents some these components, in particular at five categories which are summarized in Table 1 together with their ranges of thickness and size.

Table 1. Size ranges used in the article for typical spacecraft structures and components

S/C Component	***ts* range (mm)**	**Size range (mm)**
Tanks	0.5 – 15	150 – 500 (radius)
EOS payloads	2 – 20	500 – 1200 (side length)
Typical structures	1 – 10	100 - 2000 (side length)
Reaction wheels	0.5 – 3	70 - 150 (radius)
Battery cells	0.5 - 1	55 – 85 (radius)

The maps presented from Figure 6 through Figure 11 have all a similar structure: two materials for each map, distinguished by the dashing of the lines; two color shades, with cold colors (blues) representing the survivability and warm colors (reds) representing the demisability. The colors gradient is such that darker colors represent better solutions for both the demise and the survivability so, for example, dark blue is better than light blue for the survivability.
The Figure 6 and the Figure 7 present the maps previously described, highlighting the region where

most satellite tanks resides. The survivability part of the plots is representative of an 800 km altitude and 98 degrees inclination orbit and for a mission lifetime of 3 years, whereas the demisability analysis has been performed for an initial altitude of 120 km and an initial velocity of 7.3 km/s with an initial flight path angle of 0 degrees. In order to describe the behavior of a tank, a cylindrical shape with the diameter equal to its height was selected. Figure 6 shows the results for aluminum and stainless steel tanks. As it is possible to observe, there is a substantial difference between the two materials for both the criteria considered. The stainless steel is extremely resistant to debris impacts, indeed the 0.1% penetration probability line (dark blue dashed line) is very close to the 10% (light blue solid line) penetration probability line of the aluminum case. This means that there is a difference of two orders of magnitude in the vulnerability of two cylindrical tanks with the same dimensions but different material, i.e. aluminum or stainless steel. On the demise side, the exact opposite happens, as the aluminum configuration is more favorable with respect to the stainless steel one. It is possible to observe how the line representing the 99% RMF (orange dashed line) of the stainless steel crosses the line of the 1% RMF (red solid line) of the aluminum. This, in turn, indicates that when a cylinder made of aluminum has dimensions under the 1% line it will completely demise, whether, if it is made of stainless steel, almost all of its mass will survive.

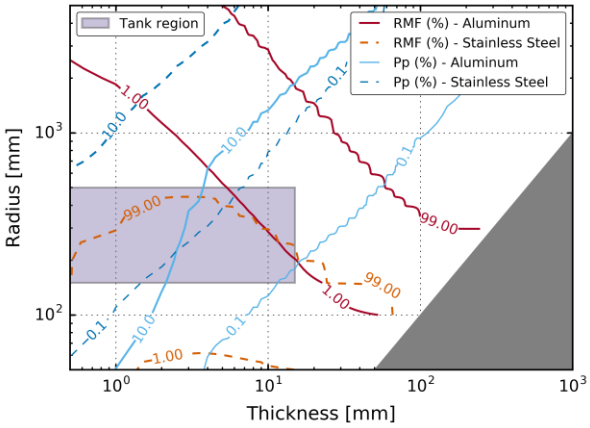

Figure 6. Survivability and demisability map for aluminum alloy and stainless steel with satellite tank region highlight

The Figure 7 shows the same map but for graphite epoxy and titanium material selection. In this case, a consistent difference between the demise behaviors of the two materials can be seen. The titanium tanks are extremely difficult to demise, due to the high melting point and heat of fusion of the titanium alloy. For this reason none of the titanium tanks analyzed fully demise, and only a small fraction (the region under the orange dashed line) suffer a partial demise. On the other extreme, the graphite epoxy components fully demise in almost all the cases analyzed. This is due to the way the graphite epoxy is modelled in DAS, that is as an equivalent material with very low heat of fusion. Such a model is used to render the charring behavior of the graphite epoxy. In fact, as the material reaches the melting temperature, it becomes very fragile and starts to char, thus making it much more demisable. This behavior is also the reason why only the 99% RMF line is represented on the graph: all the other lines almost superimpose the 99% line because the very law heat of fusion causes a very rapid demise once the melting temperature is reached.

On the survivability side, the difference is less evident but still important. As expected, the graphite epoxy is more vulnerable than the titanium alloy.

Looking at the shaded region representing common tanks dimensions, it is evident that tanks made of stainless steel will most probably survive the re-entry but they will be, at the same time, very resistant to particle impacts, at least one order of magnitude more than the other materials. On the other end, an aluminum tank will almost certainly demise but will also be much more vulnerable to debris impact. We can observe similar results for the graphite epoxy, which is more demisable with respect to aluminum but also has a higher penetration probability than the aluminum. For what concerns titanium, its resistance is higher than the one provided by aluminum and graphite epoxy but lower than the one stainless steel can provide.

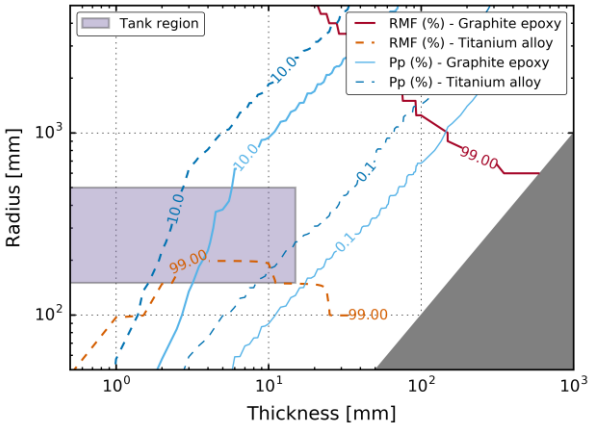

Figure 7. Survivability and demisability map for graphite epoxy and titanium alloy with satellite tank region highlight

Combining this with the fact that titanium is the least demisable among the four materials analyzed makes it the worst trade off solution.

At this point, it is important to discuss the region selected to represent cylindrical tank dimensions. The shaded area presented in Figure 6 and Figure 7 is quite extended since it covers many different options for tank

designs. Now, most of spacecraft tanks are manufactured with stainless steel and titanium; usually theses tanks have thicknesses in the order of millimeters [4, 34, 35]. However, also a sub millimeter portion is represented in the graph in order to take into account for tank liners. Liners constitute the inner part of Composite Overwrapped Pressure Vessels (COPV) and are usually under the order of millimeter in size [4, 34]. The upper limit selection results from the composite part of the COPV tanks, which is made of graphite epoxy or similar composite materials.

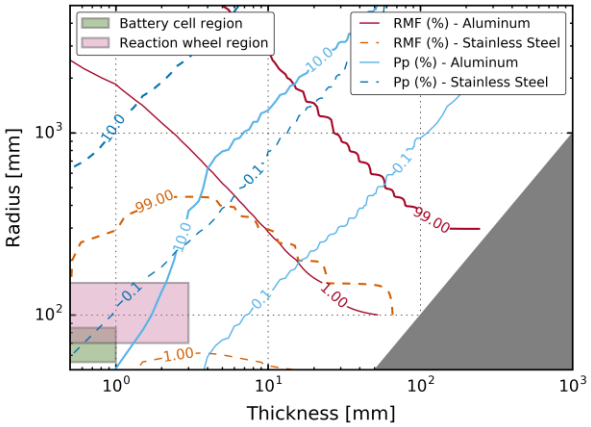

Figure 8. Survivability and demisability map for aluminium alloy and stainless steel with battery cell and reaction wheel region highlight

We present an analogous set of maps highlighting regions with a combination of radius and thickness typical of other spacecraft components. The components considered are battery cells and reaction wheels. Both objects are schematized with right cylinders (i.e. the height equals the diameter) and their regions are presented together in Figure 8 and Figure 10. The battery cell region and the reaction wheel region are represented with a green and pink area respectively.

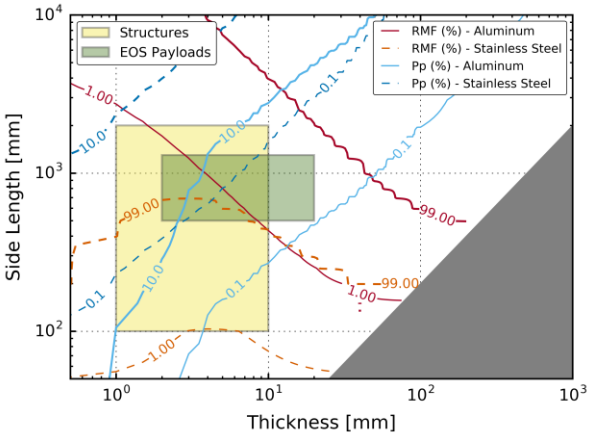

Figure 9. Survivability and demisability map for aluminium alloy and stainless steel with typical S/C structure and EOS payload region highlight

These regions were estimated looking at catalogues of battery cells [36] and reaction wheels [37, 38] manufacturers and using preliminary design relationship taken from [39]. We decided to represent these two components since they can usually survive the re-entry, thus posing risk for people on the ground. Both reaction wheels and battery cells are usually made of titanium and stainless steel; from the orange contours in Figure 8 and Figure 10 it is clear that these two materials produces non-demisable solutions.

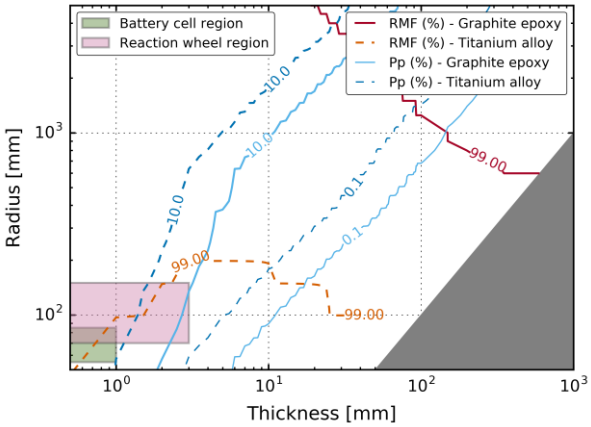

Figure 10. Survivability and demisability map for graphite epoxy and titanium alloy with battery cell and reaction wheel region highlight

In order to have demisable solutions one of the most effective solutions is to change the component material. Changing the material from steel to aluminum would make both this component demise upon re-entry. For battery cells, it is possible to consider Li-ion batteries instead of NiH and NiCd. The latter, in fact, are manufactured with stainless steel vessels whether the former are usually made of aluminum [4].

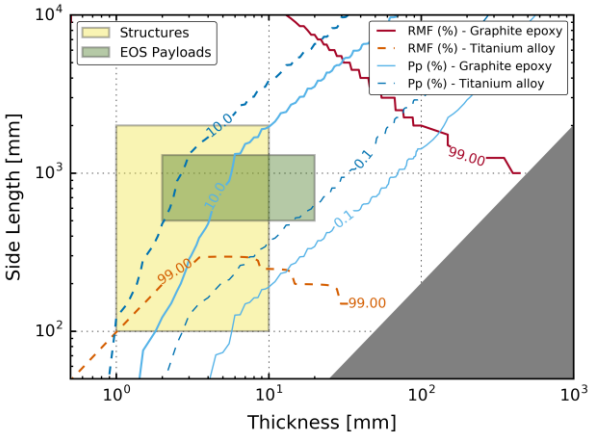

Figure 11. Survivability and demisability map for graphite epoxy and titanium alloy with typical S/C structure and EOS payload region highlight

This change of course has to come to a price in term of survivability: a more demisable aluminum battery cell will be certainly more vulnerable to debris impacts. Of course changing the material of the object is not the only option towards a more demisable configuration: considerations about the aspect ratio of the component, the position inside or outside the spacecraft are also extremely important. In addition, it is not important only for the demise but for the survivability.
It is beyond the scope of this article to investigate such possibility but they will constitute the natural development of the current work for a more detailed trade off design of spacecraft configuration for demise and survivability.
A final set of maps presented in Figure 9 and Figure 11 show the regions of dimensions for common spacecraft component and for Earth Observing System (EOS) payloads. In this case, we generated the maps for a cubic shaped structure since it better resembles the shape of common satellite structures and components such as electronic boxes and power units. The same orbital conditions have been used for the survivability analysis (800 km of altitude, 98 degrees of inclination and 3 years mission duration), as well as the same initial conditions for the demise (120 km of initial altitude, 7.3 km/s initial velocity and 0 degrees initial flight path angle). The limits for the typical spacecraft structure were taken form [35], whether the limits for the EOS payloads have been deduced from the data available for actual payloads used into NASA Earth Observing Systems Missions [40]. Their dimension were traced back to a cubic shape with equivalent volume and the range of thickness obtained assuming they were made with the lightest and heaviest material considered, i.e. graphite epoxy and stainless steel respectively. Most spacecraft structures and component casings are manufactured with aluminum. It is possible to observe that such option produces configurations that usually demise. Considering this, in most situations a configuration could be optimized by changing the geometry and the thickness of a components rather than the material itself unless specific needs for demise or survivability arises. Possibly, the most convenient option would be to switch towards a graphite epoxy configuration that provides a much better demisability, sacrificing some protection from the debris environment. This could be the case in missions where the satellites needs to have a very high rigidity such as the case of the GOCE spacecraft [41], whose primary structure is in fact made entirely from graphite epoxy.
On the payload side, the situation is much more variable since there is usually a wide variety of instruments and sensors. Their requirements and integration with the satellite are also less flexible and a change of material or geometry may be possible but not in every situation. Other options could be exploited in case of payloads.

4. MULTIOBJECTIVE OPTIMIZATION

The ultimate goal of the survivability and demise models will be their implementation into an optimization framework. The aim of this framework is to find optimized trade-off preliminary spacecraft configurations, which satisfies both the survivability and the demise requirements. In this way a more integrated approach to both this requirements can be achieved since the early stages of the mission design, thus saving late changes in the project that can lead to increased costs and delays.
A multi-objective optimization problem was formulated, whose fitness functions are represented by the criteria described in section 2.1 and 2.2. In its general formulation, a multi-objective optimization problem can be described in mathematical terms as:

$$\begin{aligned} &\mathrm{Min}\ /\ \mathrm{Max} \quad f_m(x), && m = 1,2,\ldots,M; \\ &\mathrm{Subject\ to} \quad g_j(x) \le 0, && j = 1,2,\ldots,J; \\ &\qquad\qquad h_k(x) = 0, && k = 1,2,\ldots,K; \\ &\qquad\qquad x_i^{(L)} \le x_i \le x_i^{(U)}, && i = 1,2,\ldots,n. \end{aligned} \tag{4}$$

where x is a solution vector. The first line in Eq. (4) represents the set of m objective functions, and lines two to four represent constraints to the problem in form of inequalities, equalities and boundaries respectively. In the case in exam the constraints can be represented by dimensions limitations, mass and volume upper limits, structural resistance of the component, etc.
In multi-objective optimization, there is not usually a solution that minimizes all the objective functions simultaneously. Therefore, the concept of Pareto optimality has to be introduced. A Pareto optimal solution is a solution that cannot be improved in any of the objectives functions without producing degradation in at least another objective [42]. Expressed in mathematical terms, a solution x^1 is said to Pareto dominate a second solution x^2 if:

$$\begin{aligned} &f_i(x^1) \le f_i(x^2) \ \ \forall\ i \in \{1,2,\ldots,M\} \quad \text{and} \\ &f_i(x^1) < f_i(x^2) \ \ |\exists\ j \in \{1,2,\ldots,M\} \end{aligned} \tag{5}$$

A Pareto optimal solution is a solution that is not dominated by any other solution. The set of Pareto optimal solution is referred as to the Pareto front.

In general, there is a large variety of optimization strategies. Many of these methods rely on the knowledge of the derivative of the functions to optimize. This requires the functions to have specific mathematical properties, i.e continuous functions and derivatives. For this reason they are not always applicable, especially when the problem is very complex. Other optimization strategies, such as search

algorithms, instead do not require the knowledge of the derivative of the functions. They compare the target function at points in a distance defined by a step function and move until no further improvement is found. A final set of algorithms is represented by heuristic algorithm like genetic algorithm or simulated annealing, which applies mechanisms found in nature to the optimization of a problem. In particular, genetic algorithms use the principles of natural evolution: starting with a certain population of possible solutions, they evolve it using operators like mutation, selection and crossover. The selection of the individuals in the population that carry on in the evolution depends on their quality as well as on chance. These kinds of algorithms of course rely on a certain amount of randomness both in the population generation and in the genetic operators that evolve the population itself [43, 44].

In the case in exam, the problem, in its most complex form, has to take into consideration very diversified parameters, such as the shape of the object (sphere, box, and cylinder), its dimensions and material. As it possible to observe, these parameters are a mix of discrete variables such as the material and the shape, and continuous variables like the size and thickness of the component. Considering also a future development of the project, other parameters to take into account will be the position of the component inside and outside the spacecraft and the different type of shielding options adoptable.
With all these consideration in mind, the decision to adopt a genetic algorithm was taken. Genetic algorithms were selected because of their extended documentation and their relative simplicity of implementation. Moreover they are suitable for complex problems with a combination of continuous and discrete variables such as the preliminary design of a spacecraft configuration [45]. The development of such an optimization framework is at this point of the work at its early stages, but it is intended to provide a tool for a preliminary optimization, which will take into account survivability and demise requirements since the first stages of the mission development.
The implementation of the genetic algorithm was carried out using the Python framework Distributed Evolutionary Algorithms in Python (DEAP) [46]. DEAP provides the user with a series of pre-implemented multi-objective optimization strategies such as the Non-dominated Sorting Genetic Algorithm II (NSGA II) [44] and the Strength Pareto Evolutionary Algorithm 2 (SPEA2) [47] together with a set of standard mutation and crossover operators readily available.

For the case in exam, we set up a simple optimization using the NSGAII selection mechanism provided in DEAP, selecting the Simulated Binary Bounded crossover mechanism and the Polynomial Bounded mutation operator. As is commonly done in genetic algorithms, the crossover probability was set to a high value (0.9) and the mutation probability to a low value (0.05). The initial population has 30 individuals and the evolution is carried out for just 10 generations; every generation a number of offspring equal to the initial population is generated and evaluated by the NSGAII algorithm. The individuals coming from the selection mechanism carry on further in the evolution. The number of retained individual is again equal to the size of the initial population. As mentioned before, the objective functions selected are the two criteria previously described, and expressed by Eq. (1) and Eq. (3). The search space for the optimization is bounded with the limits showed for the satellite tanks (see Table 1) with hard boundaries, and the only variables considered in the optimization were the radius and the thickness of the cylinder.

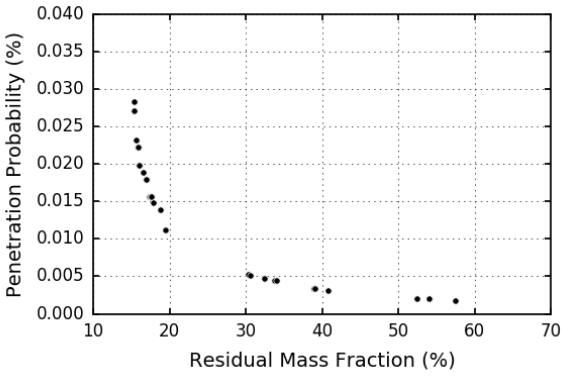

Figure 12. Pareto front

Figure 12 shows the Pareto front for the described simulation, for stainless steel tanks. Figure 13 shows the corresponding individual plotted against the correspondent survivability and demisability map. The result is what we were expecting: the optimizer identifies the solutions with the smaller diameter because, without any further constraints, it is the configuration that favors both the demise and the survivability. A smaller cylinder has less mass and it is thus more demisable, and at the same time, has a lower external surface, which in turn means a lower probability of getting hit by space debris.
The thickness on the other hand, has a maximum values that correspond to the biggest allowable thickness, which assures the highest possible survivability index. The lower value instead, in this case, does not correspond to the lower possible thickness since the highest RMF index is achieved at around 3 mm thickness. We can note that this is the value where we have the peak in the RMF contour lines for the stainless steel (see Figure 13).

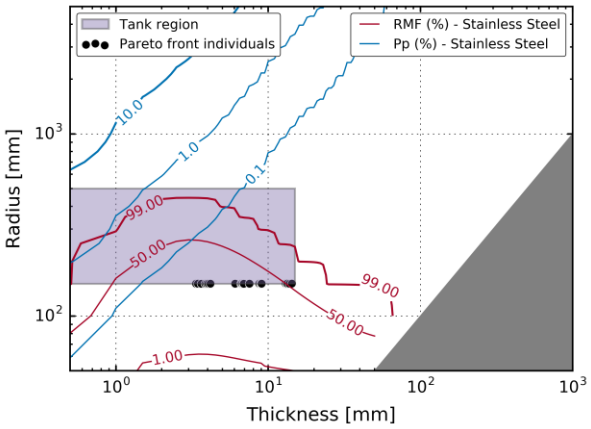

Figure 13. Pareto front individuals' survivability and demise map

5. CONCLUSIONS

A novel approach towards considering in a more integrated way the design requirements arising from the survivability and the design for demise was presented. Two models have been developed and two criteria to evaluate the level of demise and survivability have been presented. A set of maps showing simultaneously the survivability and demisability index as function of size, thickness, and material were produced. The maps shows the competing behavior of the two design requirements and have been contextualized adding satellite structures and components boundaries and considering orbit specific to Earth observation missions.
As the overall aim is to consider the two competing requirements and how they affect the preliminary design of a spacecraft, a multi-objective optimization framework looks like the natural step forward for the project. With this in mind, a preliminary optimization was performed, using as objective functions the developed criteria.

Future effort will be devoted towards the further development of the two models for the survivability and demise with the complementary objective of merging them in the outlined multi-objective optimization framework.

ACKNOWLEDGMENTS

Part of this work was funded by EPSRC DTP/CDT through the grant EP/K503150/1

REFERENCES

1. B. O'Connor 2008. Handbook for Limiting Orbital Debris. NASA Handbook 8719.14. *National Aeronautics and Space Administration, Washington, DC*.
2. F. Alby, D. Alwes, L. Anselmo *et al.* 2004. The European Space Debris Safety and Mitigation Standard. *Advances in Space Research*, 34**,** 1260-1263.
3. F. Schäfer, M. Lambert, E. Christiansen *et al.* The inter-agency space debris coordination committee (IADC) protection manual. 4th European Conference on Space Debris, 2005.
4. P. M. Waswa, and J. A. Hoffman 2012. Illustrative NASA Low Earth Orbit spacecraft subsystems design-for-demise trade-offs, analyses and limitations. *International Journal of Design Engineering*, 5**,** 21-40.
5. P. M. B. Waswa, M. Elliot, and J. A. Hoffman 2013. Spacecraft Design-for-Demise implementation strategy & decision-making methodology for low earth orbit missions. *Advances in Space Research*, 51**,** 1627-1637.
6. R. Putzar, and F. Schäfer, *Vulnerability of spacecraft equipment to space debris and meteoroids impacts*, Final Report, vol. 1, European Space Agency, 2006.
7. L. Grassi, F. Tiboldo, R. Destefanis *et al.* 2014. Satellite vulnerability to space debris – an improved 3D risk assessment methodology. *Acta Astronautica*, 99**,** 283-291.
8. E. Christiansen 2009. Handbook for Designing MMOD Protection. Huston, Texas, USA: NASA.
9. R. L. Kelley 2012. Using the Design for Demise Philosophy to Reduce Casualty Risk Due to Reentering Spacecraft.
10. M. Trisolini, H. G. Lewis, and C. Colombo. Survivability and Demise Criteria for Sustainable Spacecraft Design. International Astronautical Conference, 2015 Jerusalem.
11. NASA. 2015. *Debris Assessment Software* [Online]. NASA Orbital Debris Program Office. Available: http://orbitaldebris.jsc.nasa.gov/mitigate/das.html [Accessed July 14 2015].
12. NASA. 2009. *ORSAT* [Online]. NASA Orbital Debris Program Office. Available: http://orbitaldebris.jsc.nasa.gov/reentry/orsat.html [Accessed July 14 2015].
13. P. Omaly, and M. Spel. DEBRISK, a tool for re-entry risk analysis. ESA Special Publication, 2012. 70.
14. T. Lips, and B. Fritsche 2005. A comparison of commonly used re-entry analysis tools. *Acta Astronautica*, 57**,** 312-323.
15. R. D. Klett, *Drag Coefficients and Heating Ratios for Right Circular Cylinder in Free-Molecular and Continuum Flow from Mach 10 to 30*, Technical Report SC-RR-64-2141, Sandia Report, SC-RR-64-2141, Albuquerque, 1964.

16. W. P. Hallman, and D. M. Moody, *Trajectory Reconstruction and Heating Analysis of Columbia Composite Debris Pieces*, The Aerospace Corporation, 2005.
17. D. J. Masson, D. N. Morris, and D. E. Bloxsom, *Measurements of sphere drag from hypersonic continuum to free-molecule flow*, U.S Air Force, 1960.
18. R. Kelley, N. Hill, W. Rochelle *et al.* Comparison of ORSAT and SCARAB reentry analysis tools for a generic satellite test case. 38th COSPAR Scientific Assembly, 2010. 3931.
19. T. M. Owens. 2014. *Aero-Thermal Demise of Reentry Debris: A Computational Model.* Master of Science, Florida Insititute of Technology.
20. J. Beck. May 5 2015. *RE: Personal Communication.*
21. J. Merrifield, J. Beck, G. Markelov *et al.* Aerothermal Heating Methodology in the Spacecraft Aerothermal Model (SAM). 7th IAASS Conference, 2014.
22. J. Beck, J. Merrifield, I. Holbrough *et al.* 2015. Application of the SAM Destructive Re-Entry Code to the Spacecraft Demise Integration Test Cases. 8th European Symposium on Aerothermodynamics of Space Vehicles, March 2015 2015 Lisbon.
23. E. Minisci 2015. Space Debris and Asteroids (Re)Entry Analysis Methods and Tools. Glasgow, UK: University of Strathclyde.
24. T. Lips, V. Wartemann, G. Koppenwallner *et al.* Comparison of ORSAT and SCARAB Reentry Survival Results. 4th European Conference on Space Debris, 18-20 April 2005 Darmstadt, Germany. 533.
25. A. Tewari 2007. *Atmospheric and Space Flight Dynamics: Modeling and Simulation with MATLAB® and Simulink®*, Birkhäuser.
26. NASA 1976. U.S. Standard Atmosphere 1976. Washington, D.C.
27. R. Carmichael. Public Domain Aeronautical Software. Available: http://www.pdas.com/atmosdownload.html [Accessed March 10 2015].
28. S. Fiegel 2011. MASTER-2009 Software User Manual. Institute of Aerospace Systems (ILR).
29. N. Welty, M. Rudolph, F. Schäfer *et al.* 2013. Computational methodology to predict satellite system-level effects from impacts of untrackable space debris. *Acta Astronautica,* 88**,** 35-43.
30. J. R. Irons. 2016. *Landsat Science* [Online]. National Aeronautics and Space Administration. Available: http://landsat.gsfc.nasa.gov/ [Accessed January 2016].
31. European Space Agency. 2012. *Metop - meteorological missions* [Online]. European Space Agency. Available: http://www.esa.int/Our_Activities/Observing_the_Earth/The_Living_Planet_Programme/Meteorological_missions/MetOp/Overview14 [Accessed January 2016].
32. European Space Agency. 2014. *SPOT-6 and SPOT-7* [Online]. European Space Agency. Available: https://directory.eoportal.org/web/eoportal/satellite-missions/s/spot-6-7 [Accessed January 2016].
33. Scitor. 2016. *Space-Track.org* [Online]. Space-Track.org. Available: https://www.space-track.org/auth/login [Accessed January 2016].
34. R. H. Estes, and N. Moore 2007. An Overview of Demise Calculations, Conceptual Design Studies, and Hydrazine Compatibility Testing for the GPM Core Spacecraft Propellant Tank.
35. B. Fritsche, T. Lips, and G. Koppenwallner 2007. Analytical and numerical re-entry analysis of simple-shaped objects. *Acta Astronautica,* 60**,** 737-751.
36. EaglePicher Technologies. 2016. *Nickel-Hydrogen Batteries and Cells* [Online]. EaglePicher Technologies LLC. Available: http://www.eaglepicher.com/technologies/battery-power/nickel-hydrogen-ni-h2 [Accessed January 2016].
37. VECTRONIC Aerospace. 2014. *Space Applications* [Online]. VECTRONIC Aerospace GmbH. Available: http://www.vectronic-aerospace.com/space.php [Accessed January 2016].
38. Rockwell Collins. 2016. *Satellite Stabilization Wheels* [Online]. Rockwell Collins. Available: https://www.rockwellcollins.com/Products_and_Systems/Controls/Satellite_Stabilization_Wheels.aspx [Accessed January 2016].
39. J. R. Wertz, and W. J. Larson 1999. *Space Mission Analysis and Design*, Springer Netherlands.
40. S. Platnick. 2016. *NASA's Earth Observing System* [Online]. National Aeronautics and Space Administration. Available: http://eospso.nasa.gov/mission-category/3 [Accessed January 2016].
41. European Space Agency. 2013. *GOCE* [Online]. European Space Agency. [Accessed January 2016].
42. K. Deb 2001. *Multi-objective optimization using evolutionary algorithms*, John Wiley & Sons.

43. H.-G. Reimerdes, and W. Wohlers. Optimization of micrometeoroid and space debris protection systems. Space Debris, 2001. 655-660.
44. K. Deb, A. Pratap, S. Agarwal *et al.* 2002. A fast and elitist multiobjective genetic algorithm: NSGA-II. *Evolutionary Computation, IEEE Transactions on,* 6**,** 182-197.
45. T. Mosher 1999. Conceptual spacecraft design using a genetic algorithm trade selection process. *Journal of Aircraft,* 36**,** 200-208.
46. F. A. Fortin, F. M. De Rainville, M. A. Gardner *et al.* 2012. DEAP: Evolutionary Algorithms Made Easy. *Journal of Machine Learning Research,* 13**,** 2171-2175.
47. E. Zitzler, M. Laumanns, L. Thiele *et al.* 2001. SPEA2: Improving the strength Pareto evolutionary algorithm. Eidgenössische Technische Hochschule Zürich (ETH), Institut für Technische Informatik und Kommunikationsnetze (TIK).